Chemical Engineering Journal 494 (2024) 152733

Contents lists available at ScienceDirect

Chemical Engineering Journal

journal homepage: www.elsevier.com/locate/cej

Analytical study on the liquid–particle mass transfer coefficient for multiparticle systems

Ziming Wang [a], Charalampos Christodoulou [b], Luca Mazzei [a,*]

[a] University College London, Department of Chemical Engineering, Torrington Place, London WC1E 7JE, UK
[b] GlaxoSmithKline (GSK), Gunnels Wood Road, Stevenage SG1 2NY, UK

ARTICLE INFO

Keywords:
Liquid–particle mass transfer
Liquid–particle mass transfer coefficient
Multiparticle systems
Scaling
Order-of-magnitude analysis

ABSTRACT

This work focuses on liquid–particle mass transfer coefficient correlations for multiparticle systems. After discussing the mass transfer coefficient definitions, we review the available theoretical correlations for isolated particles and multiparticle systems. The latter are based on assumptions that are not rigorous. To estimate the mass transfer coefficient and derive a correlation for it, we apply scaling and order-of-magnitude analysis to the mass and linear momentum balance equations. The analysis features an undetermined constant. For isolated particles, we determine the value of this constant by matching the predictions of our correlation with those of other correlations available in the literature, obtaining a good fit. For multiparticle systems, we estimate the value of the constant via regression of experimental data; the predictions of our correlation align well with the experimental data, the relative percent error being less than 30% for most of the data.

1. Introduction

Multiphase flows and mass transfer between liquids and particles are present in most industrial processes, such as crystallization, absorption and extraction. Many of these processes are limited by mass transfer; therefore, to optimize them, one must estimate the mass transfer rate accurately. In general, the mass transfer rate is quantified through a mass transfer coefficient k, defined by the following equation [1]:

$$\frac{dM_t}{dt} \equiv A_t k \left(C_b - C_s\right) \tag{1}$$

where M_t and A_t are the mass and the exposed surface area of the particle, respectively, while C_b and C_s are the solute concentration in the liquid bulk and the solute concentration at saturation on the particle surface, respectively. The advantage of using k is that it can be easily estimated from the properties of the system (e.g., liquid density and particle size) and the flow variables (e.g., velocities of the particle and of the liquid), provided that correlations for k are available. In the literature, the correlations are usually expressed in dimensionless form in terms of the Sherwood number, defined as:

$$\mathrm{Sh} \equiv k d_p / D \tag{2}$$

where d_p is the particle diameter and D is the molecular diffusivity of the solute in the liquid. In general, Sh is correlated with the Reynolds number Re and the Schmidt number Sc. To find accurate correlations for Sh for both isolated particles and multiparticle systems, researchers have conducted many experimental and theoretical studies. The experimental ones usually do not offer insight into the underlying physics of mass transfer at the particle level; moreover, the correlations may be case-specific and inapplicable if experimental conditions change [2–10]. On the other hand, theoretical analyses can reveal the physics of mass transfer between the liquid and the particles at the particle scale and provide rigorous correlations; however, the precision and applicability of theoretical correlations are limited by the assumptions on which they are based [11–22].

For isolated particles, two correlations based on the concentration boundary layer theory are the most popular: the Friedlander correlation [12] is commonly used for the creeping flow regime [23,24], while the Frossling correlation [11] is commonly used for any other regime. Compared with isolated particles, multiparticle systems, such as fluidized beds, packed beds and agitated vessels, are more commonly used in industrial applications. The presence of other particles in these multiparticle systems affects the mass transfer rate for a given particle, and consequently the correlations for isolated particles do not hold. Therefore, new correlations must be derived, and these correlations are expected to feature the solid volume fraction (or equivalently the void fraction), so that the amount of solid is accounted for. However, obtaining the new correlations theoretically is difficult, and the available correlations do have their limitations. In this pursuit, researchers

* Corresponding author.
E-mail address: l.mazzei@ucl.ac.uk (L. Mazzei).

https://doi.org/10.1016/j.cej.2024.152733
Received 29 November 2023; Received in revised form 22 April 2024; Accepted 31 May 2024
Available online 1 June 2024

such as Kataoka et al. [16] and Kawase and Ulbrecht [19] studied the mass transfer process in packed beds using an analogy between packed beds and circular tubes; specifically, they applied the correlation for tubes to packed beds, characterizing the latter in terms of hydraulic diameter. Satish and Zhu [25] used the free surface model proposed by Happel [26] to quantify the velocity profile around a particle in suspensions; with this profile, they calculated the mass transfer coefficient in the same way as for isolated particles, using the concentration boundary layer theory [27]. The resulting correlation only applies to the creeping flow regime, because the free surface model holds only in this regime. Agarwal [20] assumed that the mass transfer coefficient for a single particle in packed or fluidized beds can be calculated with the correlation for isolated particles, replacing the relative velocity between the particle and the liquid by an effective velocity, denoted as u_{eff}. This velocity was also assumed to govern the drag force acting on the particles within the beds. Since correlations are available for calculating the value of this force, u_{eff} could be determined. Then, its value was used in a Frossling-type correlation. However, the use of an effective velocity is questionable, because it is well-accepted that for multiparticle systems the characteristic velocity that governs mass and momentum transfer is the interstitial velocity. Scala [22] agreed with this and replaced the relative velocity in a Frossling-type correlation with the interstitial velocity. Although Scala [22] selected the correct characteristic velocity, using it in correlations for isolated particles is still questionable. Doing this implies that the mass transfer process for a particle in a homogeneous suspension with a superficial velocity u and a void fraction ε is equivalent to that for an isolated particle with a relative liquid–particle velocity equal to u/ε. Owing to the analogy between momentum and mass transfer, this equivalency should also apply to momentum transfer; consequently, the drag force exerted on a particle in the two systems considered above should be the same. But we know that this is not true [28–31]. As we can see, except for the model by Kataoka et al. [16] and Kawase and Ulbrecht [19], the other correlations are based on the concentration boundary layer theory. To ensure that these correlations also hold when the concentration boundary layer is absent, Scala [22] added a term that accounts for mass transfer in stagnant conditions (denoted as Sh_l^0). However, a validated correlation for Sh_l^0 is still lacking [22,32–35].

In conclusion, this section acknowledges the limitations of the available correlations for mass transfer coefficients relevant to multiparticle systems. To address this issue, this study proposes a new approach for deriving these correlations, based on theoretical arguments involving scaling and order-of-magnitude analyses of mass and momentum transfer, that should offer insight into the particle-scale mass transfer process. The article is structured as follows: in Section 2, we briefly review the definitions of mass transfer coefficient and some of the correlations that are available in the literature; in Section 3, we describe our methodology and derive mass transfer coefficient correlations for multiparticle systems; finally, in Section 4, we test their validity by comparing their predictions to experimental data.

2. Review of mass transfer coefficient correlations

2.1. Isolated particles

For isolated particles, Sh is commonly correlated with other dimensionless numbers, namely Re and Sc, with similar relations. The most frequently used is [10–14,17,18,21,36]:

$$\mathrm{Sh} = 2 + C_c\,\mathrm{Re}^p\,\mathrm{Sc}^q, \quad \mathrm{Re} \equiv ud_p/\nu_e, \quad \mathrm{Sc} \equiv \nu_e/D \tag{3}$$

Here, ν_e is the kinematic viscosity of the liquid and u is the relative velocity between the particle and the liquid, which can be evaluated by various methods, including the slip-velocity theory [11,12,14,18] and the Kolmogorov theory [10,13,17,21,36]. C_c, p and q are constants; while the magnitude of Re affects the values of C_c and p, the slip-velocity theory and the Kolmogorov theory lead to different values of q. The constant 2 accounts for the mass transfer process in stagnant conditions (caused by the solute radial diffusion from or to the particle surface).

Among the available correlations, those of Friedlander [12,23] and Frossling [11], both based on the concentration boundary layer theory, are the most popular. The Friedlander correlation is used when $\mathrm{Re} \ll 1$ and $\mathrm{Pe} > 100$ [23,24], and reads:

$$\mathrm{Sh} = 0.991\,(\mathrm{Re\,Sc})^{1/3}, \quad \mathrm{Re} \ll 1, \quad \mathrm{Pe} > 100 \tag{4}$$

Here, Pe is the Peclect number, defined as:

$$\mathrm{Pe} \equiv \mathrm{Re\,Sc} = ud_p/D \tag{5}$$

This correlation was compared to the available data, and a good agreement was observed only when $\mathrm{Pe} > 100$. This is reasonable since the concentration boundary layer theory requires that Pe must be much larger than unity. To obtain a correlation that can also be used when Pe is much less than 100, one can modify Eq. (4) as follows [24]:

$$\mathrm{Sh} = 2 + 0.991\,(\mathrm{Re\,Sc})^{1/3}, \quad \mathrm{Re} \ll 1 \tag{6}$$

When $\mathrm{Pe} > 100$, adding the constant 2 to Eq. (4) causes only a slight difference, and this makes Eq. (6) applicable to any value of Pe [24]. The Frossling correlation is commonly adopted when $\mathrm{Re} \gg 1$ and reads:

$$\mathrm{Sh} = 0.552\,\mathrm{Re}^{1/2}\,\mathrm{Sc}^{1/3}, \quad \mathrm{Re} \gg 1 \tag{7}$$

In liquid–particle systems, Sc is large, and consequently when $\mathrm{Re} \gg 1$, Pe is also much larger than unity, satisfying the requirement of the concentration boundary layer theory. In addition, some researchers also add the constant 2 to this correlation to obtain the general expression of Sh shown in Eq. (3); this is acceptable since the error involved is negligible.

2.2. Multiparticle systems

2.2.1. Definitions of the mass transfer coefficient

In the literature, researchers have used two different mass transfer coefficients: the effective one k_e and the local one k_l [22,34,35,37]. Here, we clarify the difference between them. Consider a packed bed, and let its length, void fraction and specific area (that is, the area of the external surface of the particles per unit bed volume) be L, ε and a, respectively. If the superficial liquid velocity is u and the (mean) solute concentration at the axial position x along the bed is C, k_e can be defined by the following mass balance equation, subject to a boundary condition set at the inlet of the bed:

$$\begin{cases} u\dfrac{dC}{dx} = k_e a\,(C_s - C) \\ x = 0, \;\; C = C_{in} \end{cases} \tag{8}$$

where C_{in} is the solute concentration at the bed inlet. From this equation, one can obtain the concentration profile as a function of x and k_e. The value of the concentration at the outlet of the system, denoted as $C_{out} \equiv C(L)$, is given by:

$$u\,(C_{out} - C_{in}) = k_e a L\,(\Delta C)_{\ln} \tag{9}$$

where:

$$(\Delta C)_{\ln} \equiv \frac{(C_s - C_{in}) - (C_s - C_{out})}{\ln(C_s - C_{in}) - \ln(C_s - C_{out})} \tag{10}$$

Usually, C_{out} is measured experimentally, and Eq. (9) is used to calculate k_e.

At vanishingly small values of u, the concentrations at the inlet and outlet of the bed will be virtually the same owing to axial dispersion — which is present in the real system but neglected in Eq. (8); thus, from Eq. (9), also k_e is vanishingly small. However, under this condition

mass transfer occurs owing to radial diffusion, and thus the values of the local mass transfer coefficient are not vanishingly small.

To estimate the local mass transfer rate, axial dispersion in the bed must be considered in the mass balance equation for the solute; this leads to the definition of the local mass transfer coefficient k_l [22,34,37]. The mass balance equation is accordingly written as:

$$\begin{cases} u\dfrac{dC}{dx} - \varepsilon E\dfrac{d^2C}{dx^2} = k_l a\left(C_s - C\right) \\ x = 0,\ u\left(C - C_{in}\right) = \varepsilon E\dfrac{dC}{dx} \\ x = L,\ \dfrac{dC}{dx} = 0 \end{cases} \tag{11}$$

where E denotes the axial dispersion coefficient. From the equation above, one can obtain the concentration profile as a function of x and k_l. If the value of C_{out} is obtained experimentally, k_l can be calculated from the following equation:

$$\frac{C_s - C_{out}}{C_s - C_{in}} = \frac{4B\exp\left(\frac{uL}{2\varepsilon E}\right)}{(1+B)^2\exp\left(B\frac{uL}{2\varepsilon E}\right) - (1-B)^2\exp\left(-B\frac{uL}{2\varepsilon E}\right)} \tag{12}$$

where:

$$B \equiv \sqrt{1 + \frac{4ak_l\varepsilon E}{u^2}} \tag{13}$$

From Eq. (11), we see that k_l represents an average of the particle-scale mass transfer coefficient over a slice of the bed. However, it is generally assumed to be equal to the particle-scale values and can be used to validate the theoretical correlations [35,37].

2.2.2. Theoretical correlations for Sh_l

In this section, we discuss in detail the theoretical correlations for the mass transfer coefficients for multiparticle systems presented in Section 1.

To determine a correlation for the mass transfer coefficient, Kataoka et al. [16] and Kawase and Ulbrecht [19] employed the same approach used for modeling the friction factor in packed beds. In this approach, one models the system as a circular tube with a hydraulic diameter that preserves the ratio between the volume available for the flow and the total wetted surface in the packed bed; through this tube, the fluid moves at its interstitial velocity u/ε [24]. With this idealization, Kataoka et al. [16] and Kawase and Ulbrecht [19] obtained a correlation for the mass transfer coefficient in packed beds using the correlation for single-phase laminar flow in straight tubes; this resulted in the following correlation:

$$\mathrm{Sh}_l = 1.85\frac{(1-\varepsilon)^{1/3}}{\varepsilon^{2/3}}(\mathrm{Re}\,\mathrm{Sc})^{1/3},\ \mathrm{Re_p} \gg 1 \tag{14}$$

where Sh_l is defined as:

$$\mathrm{Sh}_l \equiv k_l d_p / D \tag{15}$$

In Eq. (14), Re is defined by Eq. (3) but with u representing the superficial velocity, while $\mathrm{Re_p}$ features the interstitial velocity and is defined as:

$$\mathrm{Re_p} \equiv \frac{ud_p}{\varepsilon\nu_e} \equiv \frac{\mathrm{Re}}{\varepsilon} \tag{16}$$

Note that the correlation is written in terms of Re because this is the common practice in the literature; however, the validity condition is given in terms of $\mathrm{Re_p}$ because in multiparticle systems the interstitial velocity characterizes the relative velocity between the liquid and the particles and determines the flow regime in proximity of the particles. Although this correlation (Eq. (14)) was verified by comparing it with some empirical correlations, its applicability to the whole range of variation of ε is doubtful, because when ε tends to unity, Sh_l tends to zero, while in reality it should tend to the value of the Sherwood number for an isolated particle.

Happel [26] assumed that a multiparticle system consisting of identical spherical particles can be divided into several identical cells; each cell contains a particle surrounded by a spherical fluid envelope. This is referred to as the cell model. To obtain the velocity profile of the liquid within each cell, or equivalently, in the vicinity of the particle surface, the authors simplified the mass and linear momentum balance equations under the creeping flow regime and assumed that the cell surface is frictionless. With this velocity profile, Pfeffer and Happel [15] and Zhu [38] numerically solved the solute mass balance equation within a cell, assuming that the solute concentration on the cell surface equals that in the bulk of the fluid. This allowed them to obtain the concentration profile around the particles and in turn the values of the mass transfer coefficients for various cases. However, they did not derive a correlation to calculate the mass transfer coefficient. Satish and Zhu [25] adopted the same method to obtain the velocity profile around the particles. Then, to derive a correlation for the mass transfer coefficient, they used the results of the concentration boundary layer theory applied to isolated particles in creeping flow regime [27] but replaced the velocity profile for isolated particles with that obtained from the free surface model of Happel [26]. This yielded the correlation:

$$\mathrm{Sh}_l = 1.0896\left[\frac{3\left(1-\gamma^5\right)}{2-3\gamma+3\gamma^5-2\gamma^6}\right]^{1/3}(\mathrm{Re}\,\mathrm{Sc})^{1/3},\ \mathrm{Re_p} \ll 1,\ \mathrm{Pe_p} \gg 1 \tag{17}$$

where:

$$\gamma \equiv (1-\varepsilon)^{1/3} \tag{18}$$

Here, $\mathrm{Pe_p} \equiv \mathrm{Re_p}\,\mathrm{Sc}$. Its value is required to be far larger than unity to ensure that around the particles a concentration boundary layer exists. This makes the correlation inapplicable when $\mathrm{Re_p}$ is vanishingly small.

Agarwal [20] assumed that the mass transfer coefficient of one particle in packed or fluidized beds can be calculated using the correlations for isolated particles. But in these correlations, the relative velocity between the particle and the liquid was replaced with an effective velocity u_{eff} witnessed by the particles in the bed. To relate u_{eff} to the superficial velocity and ε, the authors considered it to be the characteristic velocity governing momentum transfer and related it to the drag force via the velocity boundary layer theory. This force was also related to the dynamic pressure drop per unit length of the bed, whose dependence on the superficial velocity and ε is available in the literature. This permitted obtaining an expression for u_{eff}. Since the velocity boundary layer theory was used, this expression holds only for $\mathrm{Re_p} \gg 1$. So, the authors used the Frossling correlation, with u replaced by u_{eff}, obtaining:

$$\mathrm{Sh}_l = 0.6\left(\mathrm{Re}\frac{\omega}{\varepsilon}\right)^{2/3}\left(\frac{C_{D\varepsilon}}{8}\right)^{1/3}\mathrm{Sc}^{1/3},\ \mathrm{Re_p} \gg 1,\ \mathrm{Pe_p} \gg 1 \tag{19}$$

where:

$$C_{D\varepsilon} = \omega\left(\frac{24}{\mathrm{Re}_\varepsilon} + \frac{4}{\mathrm{Re}^{1/2}} + 0.4\right),\ \mathrm{Re}_\varepsilon = \frac{\mathrm{Re}\,\omega^3}{10.6(1-\varepsilon)^{0.7}\varepsilon^{0.3}}$$
$$\omega = \left[1 - 0.9(1-\varepsilon)^{2/3}(\varepsilon - 0.25)^{1/3}\right]^{-1} \tag{20}$$

For fluidized beds, the dynamic pressure drop per unit length of the bed is equal to the effective weight of the particles per unit volume. With this relationship, the authors calculated another expression for u_{eff} and obtained this correlation for fluidized beds:

$$\mathrm{Sh}_l = 0.6\left[\frac{\varepsilon\rho_e\left(\rho_s - \rho_e\right)d_p^3 g}{6}\right]^{1/3}\mathrm{Sc}^{1/3},\ \mathrm{Re_p} \gg 1,\ \mathrm{Pe_p} \gg 1 \tag{21}$$

where ρ_s and ρ_e are the densities of the particle and the liquid, respectively. These correlations were compared with experimental data from both liquid–particle and gas–particle systems. For the limited data used for liquid–particle systems (i.e., the systems of interest to our study), the correlations showed good agreement. However, we believe that using u_{eff} to characterize mass and momentum transfer in multiparticle systems might be doubtful, because the characteristic

velocity between the particles and the liquid should be the interstitial velocity u/ε. Scala [22] recognized this fact and adopted the interstitial velocity to replace the relative velocity in the Frossling equation. To make the correlation applicable when Re_p is vanishingly small and the concentration boundary layer is absent, the author introduced the term Sh_l^0 to account for mass transfer in stagnant conditions; the resulting correlation is:

$$Sh_l = Sh_l^0 + 0.7(Re/\varepsilon)^{1/2}\, Sc^{1/3},\ Sh_l^0 = \frac{2\,\varepsilon/\tau_t}{1-(1-\varepsilon)^{1/3}} \tag{22}$$

Here, the constant 0.7 was modified from the constant 0.552 in the Frossling equation (Eq. (7)) by fitting data. τ_t is the tortuosity of the bed; this quantity is a function of the void fraction, but Scala [22] did not provide a correlation for it. As discussed in Section 1, the mass and momentum transfer processes for a particle in a multiparticle system are not equivalent to those for isolated particles, because particle interactions do affect the values of the momentum and mass transfer coefficients. For the former (which is also referred to as drag coefficient), these interactions make a "hindrance function" appear in the correlations [21,28,39]. This term would not be present if the correlations could be obtained from those for isolated particles by simply replacing the liquid velocity with the liquid interstitial velocity. Being this true for momentum transfer, we expect it to be true also for mass transfer. Thus, we believe that their method of using the interstitial velocity in the correlation for isolated particles is unjustified. Additionally, Sh_l^0 depends on the void fraction, and this indicates that the presence of other particles can affect the mass transfer of one particle in a stagnant liquid. But this dependence is still being explored, and the current expressions require further validation. We will go into more detail about this topic in the following section.

2.2.3. *Correlations for* Sh_l^0

Experimental studies have been conducted to estimate Sh_l^0. In stagnant conditions, the values of C_{in} and C_{out} for packed beds are the same owing to axial dispersion. In this case, Eq. (12) fails to produce a value for the mass transfer coefficient. Thus, most experimental studies have measured the mass transfer coefficient at low Re, extrapolating the data to stagnant conditions. However, operating at low Re is still challenging; first, axial dispersion must be considered, and estimating the axial dispersion coefficient E may introduce uncertainty to the results; second, at low Re, the influence of free convection due to a nonuniform distribution of the solution density becomes significant; moreover, the outlet stream may be saturated owing to the long residence time of the liquid in the bed caused by the low fluid superficial velocity [35]. Given these factors, Miyauchi et al. [33] measured the mass transfer coefficient using transient pause methods at low Re conditions. On the other hand, Elgersma et al. [35] directly measured Sh_l^0 for packed beds under stagnant conditions adopting the so-called T_2-T_2 relaxation exchange NMR method. In contrast, Sørensen and Stewart [32] numerically solved the mass and linear momentum balance equations and subsequently the internal energy balance equation for systems where liquid flows through a simple cubic array of spheres, and estimated the values of the heat transfer coefficient under conditions of low Re and zero flow. Here, the heat transfer coefficient is equivalent to the mass transfer coefficient [24]. The values of Sh_l^0 for various void fractions are shown in Table 1. As we can see, the results from Elgersma et al. [35] and Sørensen and Stewart [32] are consistent, while those from Miyauchi et al. [33] deviate significantly; Elgersma et al. [35] argued that this deviation arises from the complex analysis of the data obtained by the transient pause methods. In any case, only limited data on Sh_l^0 are available, and because the values of ε are concentrated around 0.4, these data cannot capture the dependence of Sh_l^0 on ε.

There are two theoretical models available to estimate Sh_l^0. The model proposed by Scala [22] is based on the cell model, which assumes that the concentration at the cell surface is equal to that in the bulk of the liquid [15]; with this boundary condition, one can solve the solute mass balance equation at zero flow conditions to obtain the concentration profile near the surface of the particle. With this profile, Sh_l^0 can be calculated using the Fick law. But in this constitutive equation, Scala [22] used the effective diffusivity of the bed. This is an average property of the bed, whereas the mass transfer rate is quantified near the particle surface at the particle scale; therefore, we believe that the molecular diffusivity should be used. With this correction, Sh_l^0 in Eq. (22) becomes:

$$Sh_l^0 = \frac{2}{1-(1-\varepsilon)^{1/3}} \tag{23}$$

Note that when ε tends to 1, representing an isolated particle system, Sh tends to 2, consistent with the value for an isolated particle in a stagnant liquid. Another model proposed by Fedkiw and Newman [34] is based on the relationship between k_l and k_e, which was discussed above; for deep packed beds, whose ratio between the bed length and the bed diameter is large, their proposed expression for Sh_l^0 is:

$$Sh_l^0 = \frac{6\,(1-\varepsilon)\,a_1^2 E}{\varepsilon D} = 6.554\,\frac{1-\varepsilon}{\varepsilon} \tag{24}$$

where a_1 is a constant dependent on the particle positions in the bed. To obtain its value, the authors defined the axial dispersion coefficient E as D/τ_t with $\tau_t = \sqrt{2}$ and used the numerically obtained data on Sh_l^0 from Sørensen and Stewart [32] (see Table 1). Since the value of a_1 depends on the geometric condition of the bed, the last term in Eq. (24) might be inappropriate for beds where these conditions are different. Besides, Eq. (24) cannot be applied to isolated particles, because when ε tends to unity, Sh_l^0 tends to zero instead of two.

Fig. 1 illustrates the available data and theoretical models for Sh_l^0. Notice that in Eq. (22) Scala [22] did not provide a correlation for τ_t, so we used the relation by Gibilaro [40], setting $\tau_t = 1/\varepsilon$. As we see, the model proposed by Scala [22] deviates significantly from the available data; additionally, when the void fraction is small, it predicts an unexpected increase of Sh_l^0 with a rising void fraction, a trend that contradicts the behavior seen in the other models. In contrast, the model modified from Scala [22] (Eq. (23)) captures correctly the trend of how Sh_l^0 changes when the void fraction increases, the difference between its prediction and the available data being notably smaller. Comparatively, the model by Fedkiw and Newman [34] exhibits the closest alignment with the available data, but it fails to predict the expected value of $Sh_l^0 = 2$ for an isolated particle. Furthermore, the available data are quite limited, with void fractions primarily concentrated around 0.4, making it insufficient to capture the dependence of Sh_l^0 on ε. Thus, to validate the theoretical models for Sh_l^0, it is essential to conduct further experimental or numerical investigations that cover a wider range of void fractions. Once the validity of these models is determined, they can be used to explore the mass transfer coefficient for multiparticle systems in the limit of vanishingly small Re.

Table 1
Available data on Sh_l^0 for liquid–particle systems under stagnant conditions.

Reference	Sh_l^0	Voidage	Method
Miyauchi et al. [33]	16.7	~ 0.4	extrapolation from low Re
Elgersma et al. [35]	8.7 ± 0.7 9 ± 2	0.4 0.42	direct measurement
Sørensen and Stewart [32]	7.1	0.48	numerical simulation

3. Order of magnitude analysis

Here, we consider the steady-state flow of an incompressible and isothermal Newtonian liquid first around a single spherical particle and then through a homogeneous assembly of identical spherical particles.

The order of magnitude of the mass transfer coefficient k can be estimated using the following equation:

$$k\Delta C \sim D\frac{\Delta C}{\delta_c} \quad \Rightarrow \quad k \sim \frac{D}{\delta_c} \tag{25}$$

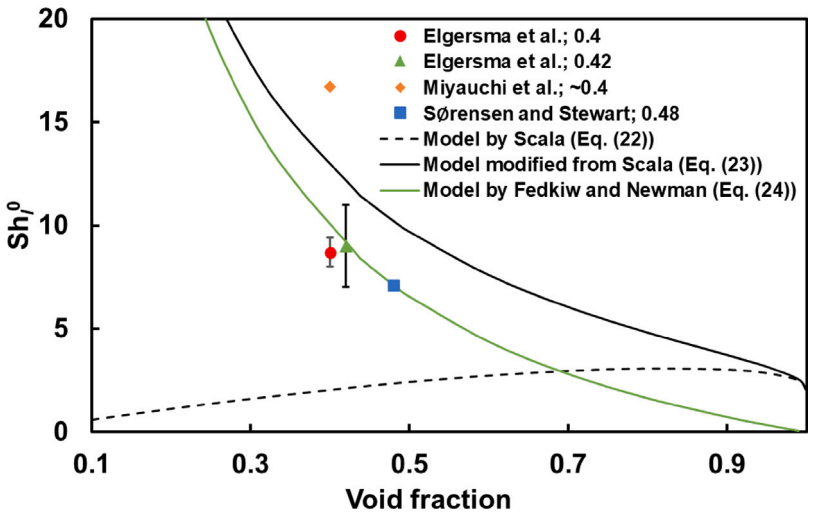

Fig. 1. Comparison between the theoretical models proposed by Fedkiw and Newman [34] (Eq. (24)) and by Scala [22] (Eq. (22), along with a modified version of the latter (Eq. (23))), and the available data of Sørensen and Stewart [32], Miyauchi et al. [33] and Elgersma et al. [35] for Sh_l^0 (the numbers in the legend are the values of the void fraction).

where ΔC is the concentration difference between the particle surface and the bulk of the liquid, and δ_c is the length scale associated with significant concentration changes around the particle (by significant we mean that the orders of magnitude of the concentration and of its change are equal). Using Eq. (2), we can estimate the order of magnitude of Sh as follows:

$$\mathrm{Sh} \equiv \frac{k d_p}{D} \sim \frac{d_p}{\delta_c} \tag{26}$$

Thus, to estimate the order of magnitude of k or Sh, one must estimate δ_c.

In liquid–particle flow systems, Sc is usually far larger than unity; consequently, unless Re is extremely small, Pe is generally far larger than unity. In these conditions, a concentration boundary layer forms around the particle surface. Since its thickness δ_c is extremely small, the curvature of the particle surface can be neglected, resulting in simplified mass balance equations for the liquid and the solute. Scaling these equations allows relating the order of magnitude of δ_c to that of the velocity scale u_c at the outer edge of the concentration boundary layer. Moreover, u_c and δ_c can be linked to the velocity and length scales for the velocity field around the particles, i.e. u_v and δ_v. Due to Sc being very large in the liquid, Pe is much larger than Re, allowing us to assume that δ_c is much smaller than δ_v. In the scaling method, it is usually assumed that the velocity profile in the vicinity of the particle surface is linear; accordingly, u_c and δ_c are related to u_v and δ_v via the following equation:

$$\frac{\delta_c}{\delta_v} \sim \frac{u_c}{u_v} \tag{27}$$

Using this and the relationship between δ_c and u_c obtained from the simplified mass balance equations, we can express δ_c as a function of δ_v and u_v, quantities that can be estimated from an order-of-magnitude analysis of the drag force. This allows using Eqs. (25) and (26) to estimate the orders of magnitude of k and Sh. Details are discussed next.

3.1. Thickness of the concentration boundary layer

In this section, we estimate the order of magnitude of δ_c for an isolated particle and relate it to u_v and δ_v. Consider a system in which an incompressible and isothermal Newtonian liquid with an approaching velocity u flows past a fixed spherical particle, and meanwhile mass transfer of solute A occurs between the particle and the liquid. The mass balance equation for the liquid in spherical coordinates reads:

$$\frac{1}{r^2}\frac{\partial r^2 u_r}{\partial r} + \frac{1}{r\sin\theta}\frac{\partial u_\theta \sin\theta}{\partial \theta} + \frac{1}{r\sin\theta}\frac{\partial u_\phi}{\partial \phi} = 0 \tag{28}$$

where u_r, u_θ and u_ϕ are the components of the velocity vector. The mass balance equation for solute A is given by:

$$\frac{\partial C_A}{\partial t} + u_r\frac{\partial C_A}{\partial r} + \frac{u_\theta}{r}\frac{\partial C_A}{\partial \theta} + \frac{u_\phi}{r\sin\theta}\frac{\partial C_A}{\partial \phi} = D_A\left[\frac{1}{r^2}\frac{\partial}{\partial r}\left(r^2\frac{\partial C_A}{\partial r}\right) + \frac{1}{r^2\sin\theta}\frac{\partial}{\partial \theta}\left(\sin\theta\frac{\partial C_A}{\partial \theta}\right) + \frac{1}{r^2\sin^2\theta}\frac{\partial^2 C_A}{\partial \phi^2}\right] \tag{29}$$

where C_A and D_A are the concentration and diffusivity of the solute in the liquid, respectively. Since in the liquid the solute is not generated, the above equation does not feature a generation term. The system of interest is at steady state; thus, the first term in Eq. (29) can be eliminated. In addition, if we assume that the flow is laminar or creeping, the flow is axisymmetric, so u_ϕ and the derivatives of the velocity components with respect to the azimuthal coordinate ϕ are zero. Furthermore, the mass transfer problem demonstrates azimuthal symmetry, which implies that $\partial C_A/\partial\phi = 0$. Then, Eqs. (28) and (29) simplify to:

$$\frac{1}{r^2}\frac{\partial r^2 u_r}{\partial r} + \frac{1}{r\sin\theta}\frac{\partial u_\theta \sin\theta}{\partial \theta} = 0 \tag{30}$$

$$u_r\frac{\partial C_A}{\partial r} + \frac{u_\theta}{r}\frac{\partial C_A}{\partial \theta} = D_A\left[\frac{1}{r^2}\frac{\partial}{\partial r}\left(r^2\frac{\partial C_A}{\partial r}\right) + \frac{1}{r^2\sin\theta}\frac{\partial}{\partial \theta}\left(\sin\theta\frac{\partial C_A}{\partial \theta}\right)\right] \tag{31}$$

The above equations can be further simplified when the concentration boundary layer exists under the condition that Pe is large [27]. First, through the order of magnitude analysis, in the tangential direction θ, mass transfer due to diffusion is negligible compared with that due to convection in the concentration boundary layer, and thus the second term in the square bracket of Eq. (31) can be neglected. Second, since the boundary layer is thin, within it the curvature due to the particle spherical shape can be neglected; accordingly, the first term on the left-hand side of Eq. (30) and the first term in the square bracket of Eq. (31) can be simplified as follows:

$$\frac{1}{r^2}\frac{\partial r^2 u_r}{\partial r} \approx \frac{\partial u_r}{\partial r},\quad \frac{D_A}{r^2}\frac{\partial}{\partial r}\left(r^2\frac{\partial C_A}{\partial r}\right) \approx D_A\frac{\partial^2 C_A}{\partial r^2} \tag{32}$$

Furthermore, we can replace the radial coordinate r with the particle radius r_p. Accordingly, the mass balance equations simplify to:

$$\frac{\partial u_r}{\partial r} + \frac{1}{r_p\sin\theta}\frac{\partial u_\theta \sin\theta}{\partial \theta} = 0 \tag{33}$$

$$u_r\frac{\partial C_A}{\partial r} + \frac{u_\theta}{r_p}\frac{\partial C_A}{\partial \theta} = D_A\frac{\partial^2 C_A}{\partial r^2} \tag{34}$$

Then, replacing r and θ by y and x, respectively, with $y \equiv r - r_p$ and $x \equiv r_p\theta$, the equations turn into:

$$\frac{\partial u_r}{\partial y} + \frac{1}{\sin\theta}\frac{\partial u_\theta \sin\theta}{\partial x} = 0 \tag{35}$$

$$u_r\frac{\partial C_A}{\partial y} + u_\theta\frac{\partial C_A}{\partial x} = D_A\frac{\partial^2 C_A}{\partial y^2} \tag{36}$$

We now scale these equations. The dimensionless variables are:

$$\overline{C}_A \equiv \frac{C_A - C_{A,b}}{C_{A,s} - C_{A,b}},\quad \overline{y} \equiv \frac{y}{\delta_c},\quad \overline{x} \equiv \frac{x}{d_p},\quad \overline{u}_r \equiv \frac{u_r}{u_{c,r}},\quad \overline{u}_\theta \equiv \frac{u_\theta}{u_{c,\theta}} \tag{37}$$

Here, $C_{A,s}$ and $C_{A,b}$ are the solute concentrations at the particle surface and in the bulk of the liquid, respectively, while $u_{c,r}$ and $u_{c,\theta}$ are the scales of the radial and tangential components of the liquid velocity, respectively. Accordingly, the dimensionless form of the continuity equation for the liquid in the concentration boundary layer is:

$$\frac{u_{c,r}}{\delta_c}\frac{\partial \overline{u}_r}{\partial \overline{y}} + \frac{u_{c,\theta}}{d_p \sin\theta}\frac{\partial \overline{u}_\theta \sin\theta}{\partial \overline{x}} = 0 \tag{38}$$

Since the derivatives in a scaled equation have unit order of magnitude, Eq. (38) yields:

$$\frac{u_{c,r}}{u_{c,\theta}} \sim \frac{\delta_c}{d_p} \tag{39}$$

The dimensionless form of the mass balance equation for solute A in the concentration boundary layer is:

$$\frac{u_{c,r}\delta_c}{D_A}\overline{u}_r\frac{\partial \overline{C}_A}{\partial \overline{y}} + \frac{u_{c,\theta}{\delta_c}^2}{D_A d_p}\overline{u}_\theta\frac{\partial \overline{C}_A}{\partial \overline{x}} = \frac{\partial^2 \overline{C}_A}{\partial \overline{y}^2} \tag{40}$$

Then, if we use Eq. (39) to eliminate $u_{c,r}$ from Eq. (40), the latter becomes:

$$\frac{u_{c,\theta}{\delta_c}^2}{D_A d_p}\left(\overline{u}_r\frac{\partial \overline{C}_A}{\partial \overline{y}} + \overline{u}_\theta\frac{\partial \overline{C}_A}{\partial \overline{x}}\right) = \frac{\partial^2 \overline{C}_A}{\partial \overline{y}^2} \tag{41}$$

from which we obtain:

$$\frac{u_{c,\theta}{\delta_c}^2}{D_A d_p} \sim 1 \quad \Rightarrow \quad \frac{\delta_c}{d_p} \sim \left(\frac{D_A}{u_{c,\theta} d_p}\right)^{1/2} \tag{42}$$

Since $u_{c,r}/u_{c,\theta} \sim \delta_c/d_p \ll 1$ (Eq. (39)), it is reasonable to assume that $u_{c,\theta}$ and u_c (that is, the order of magnitude of the fluid velocity vector) have the same order of magnitude. Thus, we can write:

$$\frac{\delta_c}{d_p} \sim \left(\frac{D_A}{u_c d_p}\right)^{1/2} \tag{43}$$

Finally, we further relate δ_c to δ_v and u_v through Eq. (27), obtaining:

$$\frac{\delta_c}{d_p} \sim \left(\frac{D_A}{u_v d_p}\frac{\delta_v}{d_p}\right)^{1/3} \tag{44}$$

3.2. Mass transfer coefficient

Using Eq. (44) in Eq. (25) or (26), we can estimate the order of magnitude of the mass transfer coefficient once δ_v and u_v are determined. In this section, we will discuss this aspect in detail for both isolated-particle and multiparticle systems. However, it is important to note that Eq. (44) is based on the concentration boundary layer theory, and thus it applies only when Pe is much larger than unity.

3.2.1. Isolated particle system

When a liquid flows around a fixed particle with an approaching velocity u, the drag force F_p exerted on this particle is given by [24]:

$$F_p = \left(\frac{\pi}{4}d_p^2\right)\left(\frac{1}{2}\rho_e u^2\right)C_D \tag{45}$$

Here, C_D is the particle drag coefficient. On the other hand, the order of magnitude of the drag force on the particle can be estimated by:

$$F_p \sim \left(\mu_e\frac{u_{v,i}}{\delta_{v,i}}\right)\pi d_p^2 \tag{46}$$

Here, μ_e is the viscosity of the liquid. The scale of the velocity field around the isolated particle, $u_{v,i}$, is the same as that of the approaching velocity u. From Eqs. (45) and (46), we can obtain the order of magnitude of the length scale characterizing the velocity gradients around the isolated particle, $\delta_{v,i}$, given by:

$$\frac{\delta_{v,i}}{d_p} \sim \frac{8}{\mathrm{Re}\,C_D} \tag{47}$$

Using Eqs. (44) and (47), with $u_{v,i} \sim u$, we can calculate the order of magnitude of the thickness of the concentration boundary layer around the isolated particle, $\delta_{c,i}$, given by:

$$\frac{\delta_{c,i}}{d_p} \sim 2\left(\frac{1}{\mathrm{Re}^2\,\mathrm{Sc}\,C_D}\right)^{1/3},\ \mathrm{Pe} \gg 1 \tag{48}$$

Using Eq. (26), the order of magnitude of Sh is given by:

$$\mathrm{Sh} \sim \frac{d_p}{\delta_{c,i}} \sim \frac{1}{2}\left(\mathrm{Re}^2\,\mathrm{Sc}\,C_D\right)^{1/3},\ \mathrm{Pe} \gg 1 \tag{49}$$

Several empirical correlations for C_D are available. In this study, we adopt that proposed by Dallavalle [41]:

$$C_D = \left(0.63 + 4.8\mathrm{Re}^{-1/2}\right)^2 \tag{50}$$

Introducing a constant C_i, expected to have unit order of magnitude, we can express Sh as:

$$\mathrm{Sh} = \frac{C_i}{2}\left(0.63\mathrm{Re} + 4.8\mathrm{Re}^{1/2}\right)^{2/3}\mathrm{Sc}^{1/3},\ \mathrm{Pe} \gg 1 \tag{51}$$

This correlation is expected to match the Friedlander correlation and the Frossling correlation within the appropriate ranges of Re. We estimated the value of C_i separately for the cases with $\mathrm{Re} \ll 1$ and $\mathrm{Re} \gg 1$. For $\mathrm{Re} \ll 1$, we used the least squares method to match Eq. (51) and the Friedlander correlation (Eq. (4)). The selected range of Re was from 0.01 to 0.1; the largest value was to satisfy the condition $\mathrm{Re} \ll 1$, while the smallest value was to ensure that $\mathrm{Pe} \gg 1$ (considering that for liquids the order of magnitude of Sc is generally 10^3). The resulting value of the constant $C_{i,1}$ is 0.682. As expected, this value has unit order of magnitude, a result that is encouraging. Thus, the resulting correlation reads:

$$\mathrm{Sh} = \frac{0.682}{2}\left(0.63\mathrm{Re} + 4.8\mathrm{Re}^{1/2}\right)^{2/3}\mathrm{Sc}^{1/3},\ \mathrm{Re} \ll 1,\ \mathrm{Pe} \gg 1 \tag{52}$$

This correlation is compared with that by Friedlander [12] in Fig. 2(a). As we can see, the match is good, with a relative percent error of less than 2%. However, as Re approaches zero, resulting in a small value of Pe and rendering the concentration boundary layer theory unusable, of course this correlation becomes invalid. To make it applicable all the way down to $\mathrm{Re} = 0$, and so for any value of Pe, as discussed in Section 2, we can modify Eq. (52) as follows:

$$\mathrm{Sh} = 2 + \frac{0.682}{2}\left(0.63\mathrm{Re} + 4.8\mathrm{Re}^{1/2}\right)^{2/3}\mathrm{Sc}^{1/3},\ \mathrm{Re} \ll 1 \tag{53}$$

Since adding the constant 2 only introduces negligible errors when $\mathrm{Pe} \gg 1$, Eq. (53) can be used for any value of Pe.

When Re is much larger than unity, we used the least squares method to match Eq. (51) and the Frossling equation (Eq. (7)). In the latter, Sh is proportional to $\mathrm{Re}^{1/2}$. Consequently, to determine accurately the value of C_i in Eq. (51), we require that:

$$\left(0.63\mathrm{Re} + 4.8\mathrm{Re}^{1/2}\right)^{2/3} \sim \mathrm{Re}^{1/2} \tag{54}$$

which can be equivalently written as:

$$0.63^2\mathrm{Re} + 2 \cdot 0.63 \cdot 4.8\mathrm{Re}^{1/2} + 4.8^2 \sim \mathrm{Re}^{1/2} \tag{55}$$

This condition is met if the term featuring $\mathrm{Re}^{1/2}$ on the left-hand side dominates over the other two terms. This occurs provided that the value of Re falls approximately between 10 and 250. With this range, the resulting value of $C_{i,2}$ is 0.469, resulting in:

$$\mathrm{Sh} = \frac{0.469}{2}\left(0.63\mathrm{Re} + 4.8\mathrm{Re}^{1/2}\right)^{2/3}\mathrm{Sc}^{1/3},\ \mathrm{Re} \gg 1,\ \mathrm{Pe} \gg 1 \tag{56}$$

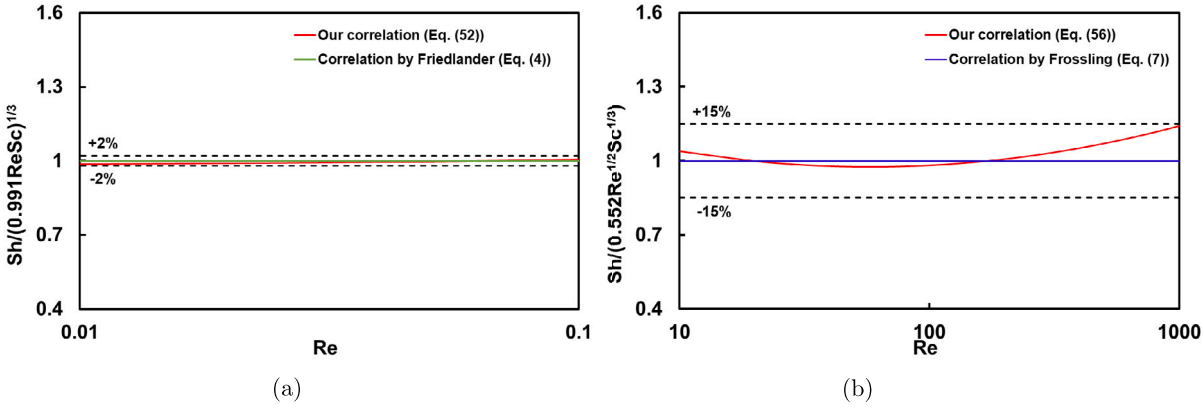

Fig. 2. Comparison of (a) Eq. (52) with the Friedlander correlation (Eq. (4)) [12], and (b) Eq. (56) with the Frossling correlation (Eq. (7)) [11].

As expected, the value of $C_{i,2}$ has unit order of magnitude. Within the designated range (i.e., $10 < \mathrm{Re} < 250$), an optimal agreement between the Frossling correlation and Eq. (56) is expected. Fig. 2(b) confirms this expectation, demonstrating a relative percent error of less than 4%. Furthermore, although deviations become more pronounced for $\mathrm{Re} > 250$, it is noteworthy that, even when Re approaches 1000, the relative percent error lies below 15%. This level of deviation is deemed acceptable.

We also attempted to determine a single value of the constant to match both the Friedlander and the Frossling correlations simultaneously. The Re ranges mentioned above ($0.01 < \mathrm{Re} < 0.1$ and $10 < \mathrm{Re} < 250$) were used and the obtained value of C_i was 0.472. As we see, this value is very close to $C_{i,2}$, because in the regression analysis, the data with larger values of Re dominate the value of the constant. As shown in the Supplementary Information (Section 2), using this value leads to a relative percent error between our correlation and that of Friedlander [12] larger than 30%. Thus, we concluded that for isolated particles using different values of the constant in different ranges of Re is preferable.

We can see that for isolated particles the estimated values of C_i have unit order of magnitude, and the derived correlations agree well with the available ones. This shows that the proposed method works correctly. Thus, we now use it for multiparticle systems.

3.2.2. Multiparticle systems

In equilibrium, the drag force acting on a particle in a uniform suspension, $F_{p,m}$, is equal to that acting on an isolated particle, F_p, because in both cases the drag force balances the effective weight force [31]. Further details on this aspect can be found in the Supplementary Information and in the work by Mazzei and Lettieri [31]. F_p features the unhindered terminal velocity u_t, and correspondingly $F_{p,m}$ is also characterized by u_t. We can write:

$$F_{p,m} = F_p = \left(\frac{\pi}{4}d_p^2\right)\left(\frac{1}{2}\rho_e u_t^2\right)C_D^t \tag{57}$$

where C_D^t denotes the particle drag coefficient characterized by u_t, which can be calculated by the Dallavalle correlation [41]:

$$C_D^t = \left(0.63 + 4.8\mathrm{Re}_\mathrm{t}^{-1/2}\right)^2,\ \mathrm{Re}_\mathrm{t} \equiv u_t d_p/\nu_e \tag{58}$$

Here, Re_t is the Reynolds number characterized by u_t. To relate the superficial velocity u to the unhindered terminal velocity u_t, we can use the empirical equations by Richardson and Zaki [42] and Rowe [43]. These respectively read:

$$u = u_t\varepsilon^n,\ n\left(\mathrm{Re}_\mathrm{t}\right) = \frac{4.8 + 2.4\cdot 0.175\mathrm{Re}_\mathrm{t}^{3/4}}{1 + 0.175\mathrm{Re}_\mathrm{t}^{3/4}} \tag{59}$$

n equals 4.8 when Re_t tends to zero and approaches 2.4 when Re_t becomes very large (values suggested by Khan and Richardson [44]). From the above equation, we can easily find that $F_{p,m}$ differs from the drag force on an isolated particle calculated by taking the relative fluid–particle velocity equal to u/ε (see Eq. (45)). This suggests that in these two systems, the momentum transfer processes are not equivalent, and so the same is expected for mass transfer. Therefore, to obtain a correlation for multiparticle systems, one cannot simply replace the relative velocity in the correlations for isolated particles with the interstitial velocity.

On the other hand, similarly to what we did in Section 3.2.1 for an isolated particle, we can estimate $F_{p,m}$ using the following equation:

$$F_{p,m} \sim \left(\mu_e\frac{u_{v,m}}{\delta_{v,m}}\right)\pi d_p^2 \tag{60}$$

Here, $u_{v,m}$ is the scale of the velocity field around the particles in the suspension; we assume its order of magnitude to be the same as that of the interstitial velocity, u/ε. $\delta_{v,m}$ is the length over which the velocity changes significantly around a particle in the suspension. Using Eqs. (57) and (60), we obtain:

$$\frac{\delta_{v,m}}{d_p} \sim \frac{8u}{\varepsilon u_t}\frac{1}{\mathrm{Re}_\mathrm{t}C_D^t} \tag{61}$$

Then, using Eqs. (58) and (59) in Eq. (61), we obtain:

$$\frac{\delta_{v,m}}{d_p} \sim \frac{8\varepsilon^{n-1}}{\mathrm{Re}_\mathrm{t}C_D^t} \sim \frac{8\varepsilon^{n-1}}{\left(0.63\mathrm{Re}^{1/2}\varepsilon^{-n/2} + 4.8\right)^2} \tag{62}$$

We now employ Eq. (44) to relate $\delta_{c,m}$ to $\delta_{v,m}$. However, Eq. (44) was derived for isolated particles; if we want to use it for multiparticle systems, we must verify that the concentration boundary layers of adjacent particles in the multiparticle system do not overlap. In other words, $\delta_{c,m}$ must be smaller than half the distance between two adjacent particles, δ_d. If we follow the cell model proposed by Pfeffer and Happel [15], we can divide the uniform suspension into non-overlapping spherical cells and estimate δ_d as the difference between the radius of the cell and the radius of the particle, given by [22]:

$$\frac{\delta_d}{d_p} = \frac{1}{2}\left[(1-\varepsilon)^{-1/3} - 1\right] \tag{63}$$

First, we compare δ_d with $\delta_{v,m}$. Their ratio is:

$$\frac{\delta_{v,m}}{\delta_d} \sim \frac{16\varepsilon^{n-1}}{\left(0.63\mathrm{Re}^{1/2}\varepsilon^{-n/2} + 4.8\right)^2\left[(1-\varepsilon)^{-1/3} - 1\right]} < \frac{16\varepsilon^{n-1}}{4.8^2\left[(1-\varepsilon)^{-1/3} - 1\right]} < \frac{16\varepsilon^{2.4-1}}{4.8^2\left[(1-\varepsilon)^{-1/3} - 1\right]} \tag{64}$$

When $\varepsilon = 0.388$, the last term in the above equation reaches its maximum value of 1.04. This implies that the order of magnitude of $\delta_{v,m}$ can be equal to or smaller than that of δ_d. As said, in liquid–particle systems the order of the magnitude of $\delta_{v,m}$ is much larger than that of $\delta_{c,m}$. So, $\delta_{c,m}$ is much smaller than δ_d and the concentration boundary

Table 2
Summary of the experimental conditions of mass transfer coefficient measurement.

Reference	Particle	Liquid	Bed	d_p (mm)	ε	Re_p	Sc	$Pe_{p/100}$
McCune and Wilhelm [2] (data from flasks are excluded)	2-naphthol modified ball-shaped pellets	water	packed bed	3.19–6.38	0.35–0.38	40–4800	1100–1510	533-70892
			fluidized bed	3.1–6.4	0.48–0.94	63–753	1204–1326	808-9688
Gaffney and Drew [3]	saliaylic and succinic acids pellets	benzol, acetone, n-butyal alcohol	packed bed	5.48–12.90	0.37–0.62	0.79–1479	159–13258	14-25206
Toshio et al. [4]	benzoic acid spheres	water	packed bed	4-6.78	0.404–0.518	2.37–366	1171–1610	33-5885
Dunn et al. [5]	lead spheres	mercury	packed bed	2.05–4.33	0.44–0.51	31–1498	123–136	42-1850
Williamson et al. [6]	benzoic acid spheres	water	packed bed	6.14–6.29	0.43–0.44	0.08–122	900–1181	0.72-1195
Wilson and Geankoplis [7]	benzoic acid spheres	water and propylene glycol solutions	packed bed	6.29	0.436	0.004–25	859–70600	0.11-1250
Upadhyay and Tripathi [8]	dished-end and flat-end benzoic cylinders	water	packed bed	5.96–11.2	0.27–0.51	3.10–3140	917–2283	28-31031
			fluidized bed	5.96–11.2	0.48–0.90	273.09–1512.60	527–1536	2332-18607
Livingston and Noble [9]	cationic resin	sodium hydroxide solution	fluidized bed	0.427–0.905	0.61–0.81	0.21–27.41	368–2896	4.3-100

* The data from flaked particles in the experiments by McCune and Wilhelm [2] are not included since their shapes are significantly different from that of spheres.

layers around adjacent particles do not overlap. Therefore, Eq. (44) holds. Then, using Eq. (62), with $u_{v,m} \sim u/\varepsilon$, we can estimate $\delta_{c,m}$ as follows:

$$\frac{\delta_{c,m}}{d_p} \sim \left(\frac{D_A}{u_{v,m}d_p}\frac{\delta_{v,m}}{d_p}\right)^{1/3} \sim 2\left(\frac{D_A}{ud_p}\frac{\varepsilon^n}{\mathrm{Re_t}C_D^t}\right)^{1/3}, \ \mathrm{Pe_p} \gg 1 \tag{65}$$

Here, $Pe_p \gg 1$ is to ensure that the concentration boundary layer around the particles in the multiparticle system exists. Finally, using Eqs. (26) and (58), and introducing a constant C_m, expected to have unit order of magnitude, we obtain:

$$\begin{aligned}\mathrm{Sh}_l &= \frac{C_m}{2}\left(\mathrm{Re_t^2}C_D^t\,\mathrm{Sc}\right)^{1/3}\\ &= \frac{C_m}{2}\left(0.63\mathrm{Re_t} + 4.8\mathrm{Re_t^{1/2}}\right)^{2/3}\mathrm{Sc}^{1/3}\\ &= \frac{C_m}{2}\varepsilon^{-2n/3}\left(0.63\mathrm{Re} + 4.8\mathrm{Re}^{1/2}\varepsilon^{n/2}\right)^{2/3}\mathrm{Sc}^{1/3},\ \mathrm{Pe_p} \gg 1\end{aligned} \tag{66}$$

This correlation applies only when the concentration boundary layer theory holds. When Pe_p is not much larger than 1 owing to vanishingly small values of Re_p, we can modify Eq. (66) as follows:

$$\mathrm{Sh}_l = \mathrm{Sh}_l^0 + \frac{C_m}{2}\varepsilon^{-2n/3}\left(0.63\mathrm{Re} + 4.8\mathrm{Re}^{1/2}\varepsilon^{n/2}\right)^{2/3}\mathrm{Sc}^{1/3} \tag{67}$$

This correlation should be used when Re_p is vanishingly small and Pe_p is not much larger than unity. However, as discussed in Section 2.2.3, the accuracy of the existing correlations for Sh_l^0 remains unvalidated. Furthermore, for isolated-particle systems with Pe much larger than unity, introducing the term that accounts for mass transfer in stagnant conditions does not change the applicability of the correlation (Eq. (53)), inasmuch as the constant 2 leads to small errors; for multiparticle systems, we will also examine whether Eq. (67) remains applicable when Pe_p is far larger than unity.

In the next section, we will use the least squares method to determine the value of C_m that minimizes the difference between predicted mass transfer coefficients and available experimental data, testing the validity of the correlations simultaneously.

4. Data analysis

To determine the value of C_m and validate the derived correlations for liquid–particle systems, we will perform regression analyses on the relevant experimental data. These experiments were carried out on packed and fluidized beds with varying values of bed void fraction and particle Reynolds number, as summarized in Table 2. Note that these data were calculated by Eq. (9) without considering axial dispersion, and so they refer to the effective mass transfer coefficient k_e. However, the local mass transfer coefficient k_l must be used to verify the correlations. Thus, these data must first be corrected to obtain the values of k_l. The correction can be carried out by establishing a relation between k_e and k_l based on Eqs. (9) and (12), given by:

$$\frac{C_s - C_{out}}{C_s - C_{in}} = \frac{4B\exp\left(\frac{uL}{2\varepsilon E}\right)}{(1+B)^2\exp\left(B\frac{uL}{2\varepsilon E}\right) - (1-B)^2\exp\left(-B\frac{uL}{2\varepsilon E}\right)}$$

$$= \exp\left(\frac{-k_e aL}{u}\right) \tag{68}$$

Here, the axial dispersion coefficient E is calculated with the model proposed by Wakao and Funazkri [37], given by:

$$E = (20 + 0.5\mathrm{Re\ Sc})\,D/\varepsilon \tag{69}$$

Note that although the discussion about k_e and k_l in Section 2.2.1 was for packed beds, the same equations apply to fluidized beds. We should also point out that Eqs. (68) and (69) are for packed beds. Nevertheless, homogeneous fluidized beds are conceptually similar to packed beds, the main difference being that in packed beds the solid volume fraction varies in a range (around 0.6) that is much smaller than in fluidized beds. Therefore, correlations valid for packed beds usually apply also to homogeneous fluidized beds (at least with good approximation). For example, originally the Ergun equation (for pressure drops) [28] was derived for packed beds, but it works well also for homogeneous fluidized beds [40] and indeed has been used to model the drag force in fluidized suspensions [45]. Furthermore, the effect of axial dispersion is important mainly when the Peclect number is small, while the values of the Peclet number for the data on fluidized beds selected in our work is large ($Pe_p > 8 \times 10^4$). Consequently, for fluidized beds the correction owing to axial dispersion is very small [37]. Thus, even if an alternative or improved correlation for the axial dispersion coefficient were employed for fluidized beds, it would yield no significant difference.

In Section 3.2.1, for isolated particles, we obtained different values of C_i when $Re \ll 1$ and $Re \gg 1$. Here, we will also obtain the values of C_m separately for $Re_p \ll 1$ ($C_{m,1}$) and $Re_p \gg 1$ ($C_{m,2}$). We now select the specific ranges for Re_p and Pe_p. Similar to the analysis conducted for isolated particles, the threshold used to determine whether Pe_p is much larger than unity is 100. Furthermore, we assume that $Re_p \gg 1$ is satisfied when Re_p is larger than 10, and $Re_p \ll 1$ is satisfied when Re_p is smaller than 0.1.

For $Re_p < 0.1$, only two data refer to values of Pe_p greater than 100, so Eq. (66) cannot be used for regression analysis. Thus, we estimate the value of $C_{m,1}$ by matching Eq. (67) to the data with $Re_p < 0.1$ and $Pe_p < 100$, and then examine whether for the data with $Re_p < 0.1$ and $Pe_p > 100$ the value obtained for the constant is applicable and whether Sh_l^0 can be included. For $Re_p > 10$, all the data refer to values of Pe_p far larger than unity (the smallest being around 2700); therefore, we can use Eq. (66) to estimate the value of $C_{m,2}$. For $0.1 < Re_p < 10$, the data also refer to values of Pe_p greater than 100, so we use Eq. (66) to match these data and obtain the value of the constant, denoted as $C_{m,3}$.

4.1. $Re_p < 0.1$

As illustrated, we use Eq. (67) to match the data with $Re_p < 0.1$ and $Pe_p < 100$ from Wilson and Geankoplis [7] and Williamson et al. [6]. However, we must first decide which value to use for Sh_l^0. The available data refer to void fraction values of 0.436 and 0.441. With these values, and in light of what we discussed in Section 2.2.3, we can reasonably take $Sh_l^0 = 8.0$. Using the least squares regression

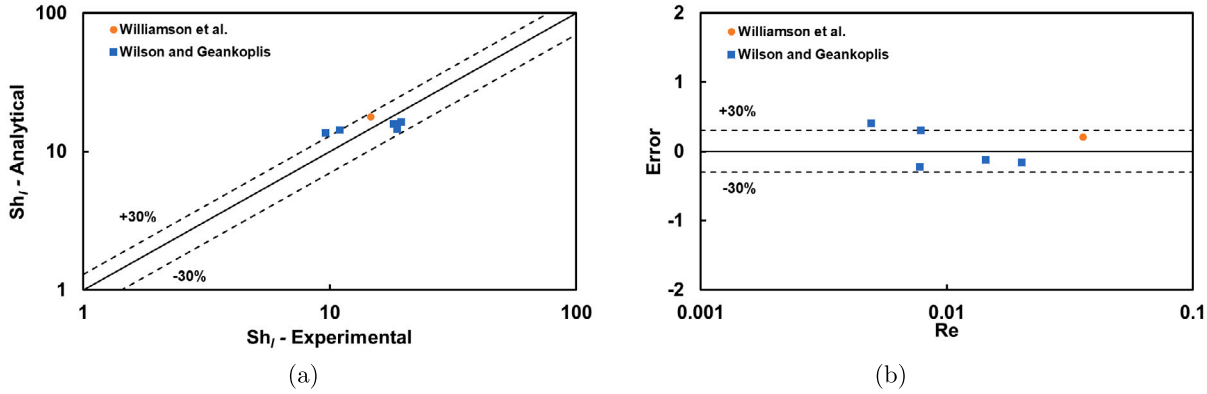

Fig. 3. (a) Comparison between the predictions of Eq. (67) with $C_{m,1} = 0.594$ and $Sh_l^0 = 8.0$ and the experimental data of Williamson et al. [6] and Wilson and Geankoplis [7]. (b) Relative percent error between them at various Re for $Re_p < 0.1$ and $Pe_p < 100$.

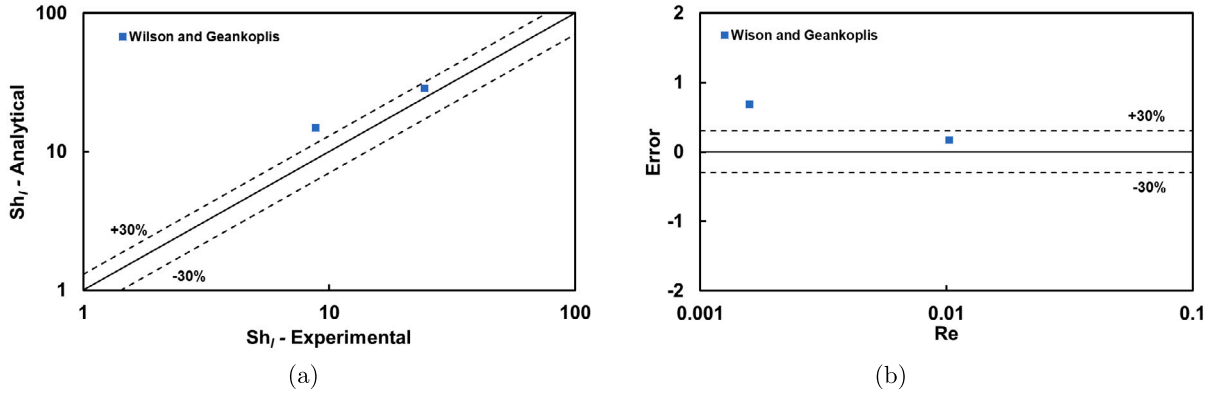

Fig. 4. (a) Comparison between the predictions of Eq. (66) with $C_{m,1} = 0.594$ and the experimental data of Wilson and Geankoplis [7]. (b) Relative percent error between them at various Re for $Re_p < 0.1$ and $Pe_p > 100$.

analysis, we estimate the value of $C_{m,1}$ to be 0.594. As expected, it has unit order of magnitude. Using this value, in Fig. 3 we compare the predicted values of Sh_l with the experimental data; the relative percent error between most of them lies within 30%. However, to make this correlation applicable to other values of the void fraction, one should have a reliable equation relating Sh_l^0 to the void fraction. As discussed, such an equation is still lacking.

Next, we compare Eq. (67) with $C_{m,1} = 0.594$ to the two data with $Re_p < 0.1$ and $Pe_p > 100$ from Wilson and Geankoplis [7]. Since these data refer to a void fraction of 0.436, we can still take $Sh_l^0 = 8.0$. But this correlation overestimates the value of the Sherwood number (the results are not reported), indicating that including Sh_l^0 when $Pe_p > 100$ introduces an appreciable error, at least for these data. Excluding Sh_l^0, in Fig. 4 we compare the values predicted by Eq. (66) with $C_{m,1} = 0.594$ to the experimental data. The relative percent error is around 30%. This can possibly be explained by the following factors: on the one hand, the amount of data used for the regression analysis is small; on the other hand, as discussed in Section 2.2.3, measurement of the mass transfer coefficient when Re_p is small is challenging, and the available experimental data may be inaccurate [35]. Furthermore, when $Pe_p < 100$, assuming $Sh_l^0 = 8.0$ at the given values of the void fraction may also be inaccurate.

4.2. $Re_p > 10$, $Pe_p > 100$

Using Eq. (66) to match the experimental data with $Re_p > 10$ and $Pe_p > 100$ from Wilson and Geankoplis [7], Williamson et al. [6], McCune and Wilhelm [2], Gaffney and Drew [3], Dunn et al. [5], Upadhyay and Tripathi [8], Toshio et al. [4], and Livingston and Noble [9], we estimate $C_{m,2}$ to be 0.437. With this value, in Fig. 5 we compare the predictions of Eq. (66) with the experimental data. In the Supplementary Information, we also report the predicted and measured values of the Chilton–Colburn factor as a function of Re for various values of the void fraction, which can help us illustrate the dependence of the mass transfer coefficient on the void fraction. The results indicate that for most of the data, over a broad range of Re values, the relative percent error is less than 30%. However, as shown in Fig. 5(b), for most of the data related to fluidized beds and obtained from the experiments of Upadhyay and Tripathi [8], the values of the Sherwood number are underestimated by more than 30%. This might be caused by the following factors. On the one hand, these researchers used cylinders with dished and flat ends rather than spherical particles. On the other hand, in their experiments the ratio between the bed and particle diameters is small; consequently, the wall effect is significant, making the liquid velocity and void fraction profiles be nonuniform [46]. In contrast, the correlations derived in our study are based on uniform suspensions.

4.3. $0.1 < Re_p < 10$

Using Eq. (66) to match the experimental data with $0.1 < Re_p < 10$ from Wilson and Geankoplis [7], Williamson et al. [6], Upadhyay and Tripathi [8], Gaffney and Drew [3], Toshio et al. [4], and Livingston and Noble [9], we estimate the value of $C_{m,3}$ to be 0.568. With this value, in Fig. 6 we compare the predicted values of Sh_l with the experimental data. In the Supplementary Information, we also report the predicted and measured values of the Chilton–Colburn factor as a function of Re for various values of the void fraction. For most data, the relative percent error is less than 30%, except for the data of Livingston

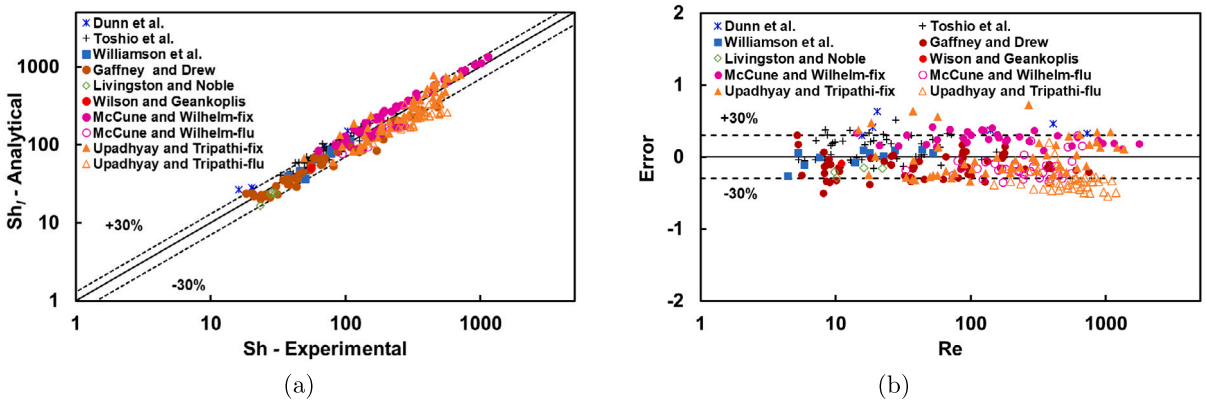

Fig. 5. (a) Comparison between the predictions of Eq. (66) with $C_{m,2} = 0.437$ and the experimental data of Wilson and Geankoplis [7], Williamson et al. [6], McCune and Wilhelm [2], Gaffney and Drew [3], Dunn et al. [5], Upadhyay and Tripathi [8], Toshio et al. [4], and Livingston and Noble [9]. (b) Relative percent error between them at various Re for $Re_p > 10$ and $Pe_p > 100$ (in the legends, 'fix' and 'flu' stand for fixed and fluidized bed, respectively).

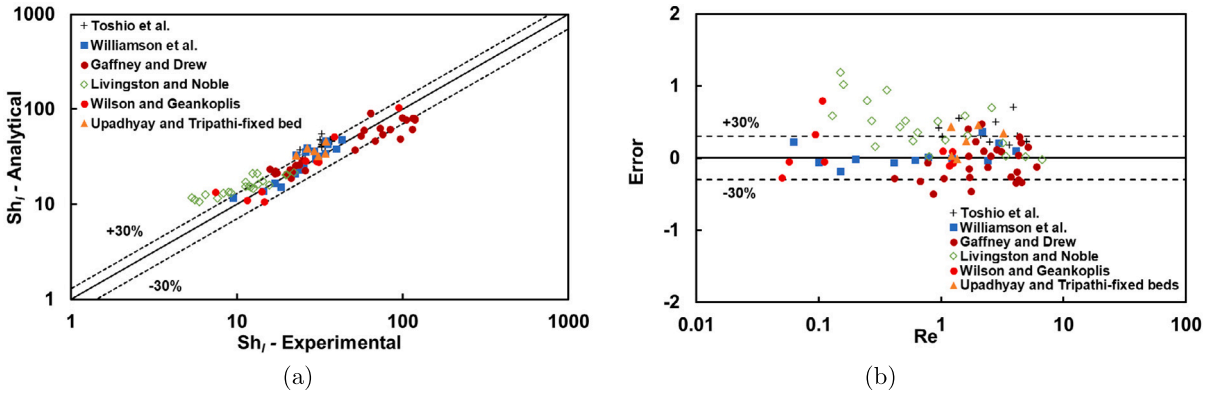

Fig. 6. (a) Comparison between the predictions of Eq. (66) with $C_{m,3} = 0.568$ and the experimental data of Wilson and Geankoplis [7], Williamson et al. [6], Upadhyay and Tripathi [8], Gaffney and Drew [3], Toshio et al. [4], and Livingston and Noble [9]. (b) Relative percent error between them at various Re for $0.1 < Re_p < 10$ and $Pe_p > 100$.

and Noble [9]. But these refer to small values of Re, and, as discussed in Section 4.1, many factors may make these data unreliable.

In the limit of $\varepsilon \to 1$, the correlations for multiparticle systems are expected to reduce to those for isolated particles. In Fig. 7, we compare the results of our correlations for $\varepsilon = 1$ with those of the correlations by Friedlander [12] and Frossling [11], observing that for the Friedlander equation the deviation is less than 15%, while for the Frossling equation it is within 10%. This further supports the validity of our correlations. The larger deviation between the predictions of our correlation and those of the Friedlander equation, compared to the deviation reported in Fig. 2 for isolated particle systems, is probably caused by the few experimental data used in the calculation of $C_{m,1}$. In the Supplementary Information, we also compare the predictions of the correlations discussed in Section 2.2.2 to the experimental data. For $Re_p < 0.1$ and $Pe_p > 100$, the free surface model (Eq. (17)) performs slightly less well than our model. For $Re_p > 10$ and $Pe_p > 100$, the equation of Kataoka et al. [16] and Kawase and Ulbrecht [47] (Eq. (14)) deviates significantly from the experimental data for $Re > 100$. For the correlations proposed by Agarwal [20], we considered only Eq. (19), since Eq. (21) is restricted to fluidized beds. For $Re_p > 10$ and $Pe_p > 100$, Eq. (19) aligns well with the experimental data with only a slight overestimation. Finally, the values predicted by the correlation proposed by Scala [22] (Eq. (22)) are examined. As discussed in Section 2.2.3, we set τ_t to be $1/\varepsilon$. The results reveal a noticeable underestimation for some of the data. When we implement the modification of Sh_l^0 as specified in Eq. (23), the underestimation when Re is small reduces, but for large Re remains notable. This behavior is consistent with the influence of Sh_l^0 being greater at smaller Re values.

We can see that the value of the constant C_m varies for different ranges of Re_p, but it always has unit order of magnitude. This is as much as one can expect, because our correlations were obtained by order-of-magnitude analysis. Because the estimated values of C_m are close, we tried to correlate all the experimental data where $Pe_p \gg 1$ with just one value. This resulted in $C_m = 0.427$. This value is close to that of $C_{m,2}$, for the amount of data with $Re_p > 10$ is large, so these data dominate the value of the constant. As we see in the Supplementary Information, the predictions based on this value are still acceptable. We also used this value in Eq. (67) (with $Sh_l^0 = 8.0$) to match the data with $Pe_p < 100$, obtaining good results. However, when $\varepsilon = 1$ and $Re_p \ll 1$, the relative percent error between our correlation and that of Friedlander exceeds 30%. The figures for these comparisons are in the Supplementary Information. In light of these results, similarly to isolated particles, we conclude that for multiparticle systems, using different values of the constant is preferable, because this makes the correlations more accurate.

5. Conclusions

We derived mass transfer coefficient correlations for isolated particles and multiparticle systems, using scaling and order-of-magnitude arguments. We estimated the mass transfer coefficient as the ratio between the molecular diffusivity and the thickness δ_c of the concentration boundary layer. To estimate the latter, we scaled the continuity equation and the mass balance equation for the solute, relating δ_c to the length and velocity scales of the fluid velocity field around the particle. These scales were estimated via an order-of-magnitude

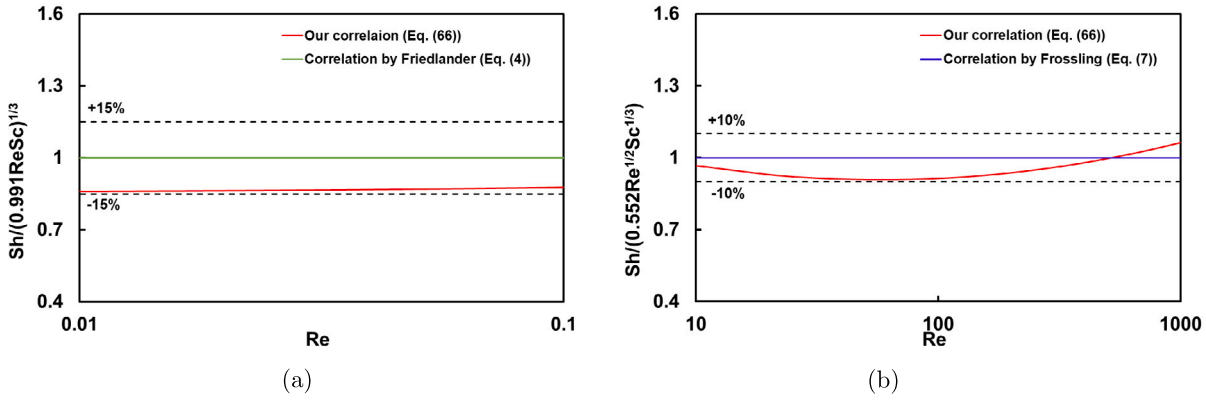

Fig. 7. Comparison, for $\varepsilon = 1$, between (a) Eq. (66) with $C_{m,1} = 0.594$ and the Friedlander correlation (Eq. (4)) [12] and (b) Eq. (66) with $C_{m,2} = 0.437$ and the Frossling correlation (Eq. (7)) [11].

analysis on the drag force, using information available for isolated particles and multiparticle systems. With δ_c known, we obtained the mass transfer coefficient correlations. These featured an undetermined constant of unit order of magnitude. For isolated particles, we found the value of this constant by matching our correlation with those of Friedlander and Frossling. Within the appropriate range of Re, the relative percent error between our correlation and that of Friedlander lies within 2%, while for that of Frossling the error is within 15%. For multiparticle systems, the constant was estimated by regression analysis of the available experimental data. The resulting correlation aligns well with the experimental data, with the relative percent error between the predicted and measured values being less than 30% for most of the data, in many cases being more accurate than the other correlations examined in this study. Moreover, unlike many available correlations, whose validity is restricted to specific ranges of Re, our correlation is valid over a large range of Re, spanning several orders of magnitude; the only thing that should be changed (to obtain better accuracy) is the value of the single undetermined constant present in the correlation (which, however, is known to have unit order of magnitude), but the functional form of the correlation is unchanged. Finally, being based on the classical approach of scaling and order-of-magnitude analysis applied to the fundamental equations of change, our method rests on solid scientific arguments, offering valuable insight into the investigated process.

Notation

a	specific area of the packed bed	1/m
a_1	model constant	–
A_t	surface area of the particle	m^2
C	solute concentration	kg/m^3
C_A	concentration of solute A	kg/m^3
$\overline{C}_A$	dimensionless concentration of solute A	–
$C_{A,b}$	concentration of solute A in the liquid bulk	kg/m^3
$C_{A,s}$	concentration of solute A at saturation	kg/m^3
C_b	solute concentration in the liquid bulk	kg/m^3
C_c	model constant	–
C_D	particle drag force coefficient	–
C_D^t	particle drag force coefficient	–
$C_{D\varepsilon}$	constitutive function	–
C_i	model constant	–
$C_{i,1}$	model constant	–
$C_{i,2}$	model constant	–
C_{in}	solute concentration at the bed inlet	kg/m^3
C_m	model constant	–
$C_{m,1}$	model constant	–
$C_{m,2}$	model constant	–
C_{out}	solute concentration at the bed outlet	kg/m^3
C_s	solute concentration at saturation	kg/m^3
d_p	particle diameter	m
D	diffusivity of the solute	m^2/s
D_A	diffusivity of the solute A	m^2/s
E	axial dispersion coefficient	m^2/s
F_p	drag force on an isolated particle	$kg\,m/s^2$
$F_{p,m}$	drag force on a particle in a multiparticle system	$kg\,m/s^2$
g	magnitude of the gravitational acceleration	m/s^2
k	mass transfer coefficient	m/s
k_e	effective mass transfer coefficient	m/s
k_l	local mass transfer coefficient	m/s
L	length of the packed bed	m
M_t	mass of the particle	kg
n	Richardson–Zaki exponent	–
p	model constant	–
Pe	Peclect number	–
Pe_p	particle Peclect number	–
q	model constant	–
Re	Reynolds number	–
Re_p	particle Reynolds number	–
Re_t	Reynolds number	–
Re_ε	constitutive function	–
r_p	particle radius	m
Sc	Schmidt number	–
Sh	Sherwood number	–
Sh_l	local Sherwood number	–
Sh_l^0	local Sherwood number in stagnant conditions	–
t	time	s
u	superficial velocity	m/s
u_c	velocity scale for the concentration change around particles	m/s
$u_{c,i}$	velocity scale for the concentration change around isolated particles	m/s
$u_{c,m}$	velocity scale for the concentration change around a particle in a multiparticle system	m/s
$u_{c,r}$	scale of the radial component of the liquid velocity	m/s
$u_{c,\theta}$	scale of the tangential component of the liquid velocity	m/s
u_{eff}	effective velocity	m/s
u_r	velocity in r direction	m/s
$\overline{u}_r$	dimensionless velocity in r direction	–
u_t	unhindered terminal velocity	m/s
u_v	velocity scale for the velocity field around particles	m/s
$u_{v,i}$	velocity scale for the velocity field around isolated particles	m/s
$u_{v,m}$	velocity scale for the velocity field around a particle in a multiparticle system	m/s
u_θ	velocity in θ direction	m/s
$\overline{u}_\theta$	dimensionless velocity in θ direction	–
u_ϕ	velocity in ϕ direction	m/s

Greek symbols

γ	constitutive function	–
δ_c	length scale for the concentration change around particles	m

$\delta_{c,i}$	length scale for the concentration change around isolated particles	m
$\delta_{c,m}$	length scale for the concentration change around a particle in a multiparticle system	m
δ_d	half the distance between two adjacent particles	m
δ_v	length scale for the velocity field around particles	m
$\delta_{v,i}$	length scale for the velocity field around isolated particles	m
$\delta_{v,m}$	length scale for the velocity field around a particle in a multiparticle system	m
ϵ	void fraction	–
μ_e	shear viscosity of the liquid	kg/m s
ν_e	kinematic viscosity of the liquid	m^2/s
ρ_e	mass density of the liquid	kg/m^3
ρ_s	mass density of the particle	kg/m^3
τ_t	tortuosity of the bed	–
ω	constitutive function	–

CRediT authorship contribution statement

Ziming Wang: Writing – review & editing, Writing – original draft, Visualization, Validation, Software, Methodology, Formal analysis, Data curation, Conceptualization. **Charalampos Christodoulou:** Writing – review & editing, Supervision, Project administration, Funding acquisition. **Luca Mazzei:** Writing – review & editing, Supervision, Resources, Project administration, Methodology, Investigation, Funding acquisition, Formal analysis, Conceptualization.

Declaration of competing interest

The authors declare the following financial interests/personal relationships which may be considered as potential competing interests: Luca Mazzei reports financial support was provided by GlaxoSmithKline (GSK). Luca Mazzei reports a relationship with GlaxoSmithKline (GSK) that includes: funding grants. If there are other authors, they declare that they have no known competing financial interests or personal relationships that could have appeared to influence the work reported in this paper.

Data availability

Data will be made available on request.

Acknowledgments

Funding from GlaxoSmithKline, UK is gratefully acknowledged.

Appendix A. Supplementary data

Supplementary material related to this article can be found online at https://doi.org/10.1016/j.cej.2024.152733.

References

[1] A.A. Noyes, W.R. Whitney, The rate of solution of solid substances in their own solutions, J. Am. Chem. Soc. 19 (12) (1897) 930–934.
[2] L.K. McCune, R.H. Wilhelm, Mass and momentum transfer in a solid-liquid system, Ind. Eng. Chem. Res. 41 (6) (1949) 1124–1134.
[3] B.J. Gaffney, T.B. Drew, Mass transfer from packing to organic solvents in single phase flow through a column, Ind. Eng. Chem. Res. 42 (6) (1950) 1120–1127.
[4] I. Toshio, D. Ohtake, T. Okada, Mass transfer in packed bed, Chem. Mach. 15 (6) (1951) 255–261.
[5] W.E. Dunn, C.F. Bonilla, C. Ferstenberg, B. Gross, Mass transfer in liquid metals, AIChE J. 2 (2) (1956) 184–189.
[6] J.E. Williamson, K.E. Bazaire, C.J. Geankoplis, Liquid-phase mass transfer at low Reynolds numbers, Ind. Eng. Chem. Fundam. 2 (2) (1963) 126–129.
[7] E.J. Wilson, C.J. Geankoplis, Liquid mass transfer at very low Reynolds numbers in packed beds, Ind. Eng. Chem. Fundam. 5 (1) (1966) 9–14.
[8] S.N. Upadhyay, G. Tripathi, Liquid-phase mass transfer in fixed and fluidized beds of large particles, J. Chem. Eng. Data 20 (1) (1975) 20–26.
[9] A.G. Livingston, J.B. Noble, Mass transfer in liquid-solid fluidized beds of ion exchange resins at low Reynolds numbers, Chem. Eng. Sci. 48 (6) (1993) 1174–1178.
[10] E.Y. Bong, N. Eshtiaghi, J. Wu, R. Parthasarathy, Optimum solids concentration for solids suspension and solid–liquid mass transfer in agitated vessels, Chem. Eng. Res. Des. 100 (2015) 148–156.
[11] N. Frossling, Uber die verdunstung fallernder tropfen, Gerlands Beitr. Geophys. 52 (1938) 170–216.
[12] S. Friedlander, Mass and heat transfer to single spheres and cylinders at low Reynolds numbers, AIChE J. 3 (1) (1957) 43–48.
[13] P.H. Calderbank, M.B. Moo-Young, The continuous phase heat and mass-transfer properties of dispersions, Chem. Eng. Sci. 16 (1–2) (1961) 39–54.
[14] P. Harriott, Mass transfer to particles: Part I. Suspended in agitated tanks, AIChE J. 8 (1) (1962) 93–101.
[15] R. Pfeffer, J. Happel, An analytical study of heat and mass transfer in multiparticle systems at low Reynolds numbers, AIChE J. 10 (5) (1964) 605–611.
[16] T. Kataoka, H. Yoshida, K. Ueyama, Mass transfer in laminar region between liquid and packing material surface in the packed bed, J. Chem. Eng. Japan 5 (2) (1972) 132–136.
[17] D.M. Levins, J.R. Glastonbury, Application of Kolmogorofff's theory to particle-liquid mass transfer in agitated vessels, Chem. Eng. Sci. 27 (3) (1972) 537–543.
[18] R. Kuboi, I. Komasawa, T. Otake, M. Iwasa, Fluid and particle motion in turbulent dispersion-III: Particle-liquid hydrodynamics and mass-transfer in turbulent dispersion, Chem. Eng. Sci. 29 (3) (1974) 659–668.
[19] Y. Kawase, J.J. Ulbrecht, A new approach for heat and mass transfer in granular beds based on the capillary model, Ind. Eng. Chem. Fundam. 24 (1) (1985) 115–116.
[20] P.K. Agarwal, Transport phenomena in multi-particle systems-II. Particle-fluid heat and mass transfer, Chem. Eng. Sci. 43 (9) (1988) 2501–2510.
[21] J.T. Davies, Particle suspension and mass transfer rates in agitated vessels, Chem. Eng. Process. 20 (4) (1986) 175–181.
[22] F. Scala, Particle-fluid mass transfer in multiparticle systems at low Reynolds numbers, Chem. Eng. Sci. 91 (2013) 90–101.
[23] S.K. Friedlander, A note on transport to spheres in Stokes flow, AIChE J. 7 (2) (1961) 347–348.
[24] R.B. Bird, W.E. Stewart, E.N. Lightfoot, Transport Phenomena, John Wiley & Sons, 2002.
[25] M.G. Satish, J. Zhu, Flow resistance and mass transfer in slow non-Newtonian flow through multiparticle systems, J. Appl. Mech. 59 (1992) 431–437.
[26] J. Happel, Viscous flow in multiparticle systems: Slow motion of fluids relative to beds of spherical particles, AIChE J. 4 (2) (1958) 197–201.
[27] L.A. Belfiore, Transport Phenomena for Chemical Reactor Design, John Wiley & Sons, 2003.
[28] S. Ergun, Fluid flow through packed columns, Chem. Eng. Prog. 48 (1952) 89–94.
[29] C.Y. Wen, Y.H. Yu, Mechanics of fluidization, Chem. Eng. Prog. Symp. Ser. 62 (1966) 100–111.
[30] R. Di Felice, The voidage function for fluid-particle interaction systems, Int. J. Multiph. Flow 20 (1) (1994) 153–159.
[31] L. Mazzei, P. Lettieri, A drag force closure for uniformly dispersed fluidized suspensions, Chem. Eng. Sci. 62 (22) (2007) 6129–6142.
[32] J.P. Sørensen, W.E. Stewart, Computation of forced convection in slow flow through ducts and packed beds-III. Heat and mass transfer in a simple cubic array of spheres, Chem. Eng. Sci. 29 (3) (1974) 827–832.
[33] T. Miyauchi, K. Matsumoto, T. Yoshida, Liquid film coefficient of mass transfer in low Peclet number region for sphere packed beds, J. Chem. Eng. Japan 8 (3) (1975) 228–232.
[34] P. Fedkiw, J. Newman, Low Peclet number behavior of the transfer rate in packed beds, Chem. Eng. Sci. 33 (8) (1978) 1043–1048.
[35] S.V. Elgersma, A.J. Sederman, M.D. Mantle, L.F. Gladden, Measuring the liquid-solid mass transfer coefficient in packed beds using T2-T2 relaxation exchange NMR, Chem. Eng. Sci. 248 (2022) 117229.
[36] P.M. Armenante, D.J. Kirwan, Mass transfer to microparticles in agitated systems, Chem. Eng. Sci. 44 (12) (1989) 2781–2796.
[37] N. Wakao, T. Funazkri, Effect of fluid dispersion coefficients on particle-to-fluid mass transfer coefficients in packed beds: Correlation of Sherwood numbers, Chem. Eng. Sci. 33 (10) (1978) 1375–1384.
[38] J. Zhu, Convective and conductive heat transfer of creeping flow in a multi-particle system, Int. J. Therm. Sci. 159 (2021) 106573.
[39] P. Lettieri, L. Mazzei, Challenges and issues on the CFD modeling of fluidized beds: A review, J. Comput. Multiph. Flows 1 (2) (2009) 83–131.
[40] L. Gibilaro, Fluidization Dynamics, Elsevier, 2001.
[41] J.M. Dallavalle, Micromeritics: The Technology of Fine Particles, Pitman, London, 1948.
[42] J.F. Richardson, W.N. Zaki, Sedimentation and fluidization: Part I, Trans. Insti. Chem. Eng. 32 (1954) 35–53.
[43] P.N. Rowe, A convenient empirical equation for estimation of the Richardson-Zaki exponent, Chem. Eng. Sci. 42 (1987) 2795–2796.

[44] A.R. Khan, J.F. Richardson, Fluid-particle interactions and flow characteristics of fluidized beds and settling suspensions of spherical particles, Chem. Eng. Commun. 78 (1) (1989) 111–130.
[45] D. Gidaspow, Multiphase flow and fluidization, Academic Press, 1994.
[46] H. Martin, Low Peclet number particle-to-fluid heat and mass transfer in packed beds, Chem. Eng. Sci. 33 (7) (1978) 913–919.
[47] Y. Kawase, J.J. Ulbrecht, Drag and mass transfer in non-Newtonian flows through multi-particle systems at low Reynolds numbers, Chem. Eng. Sci. 36 (7) (1981) 1193–1202.